Robust Image Watermarking Based on Multiband Wavelets and Empirical Mode Decomposition

Ning Bi, Qiyu Sun, Daren Huang, Zhihua Yang, and Jiwu Huang

***Abstract*—In this paper, we propose a blind image watermarking algorithm based on the multiband wavelet transformation and the empirical mode decomposition. Unlike the watermark algorithms based on the traditional two-band wavelet transform, where the watermark bits are embedded directly on the wavelet coefficients, in the proposed scheme, we embed the watermark bits in the mean trend of some middle-frequency subimages in the wavelet domain. We further select appropriate dilation factor and filters in the multiband wavelet transform to achieve better performance in terms of perceptually invisibility and the robustness of the watermark. The experimental results show that the proposed blind watermarking scheme is robust against JPEG compression, Gaussian noise, salt and pepper noise, median filtering, and ConvFilter attacks. The comparison analysis demonstrate that our scheme has better performance than the watermarking schemes reported recently.**

***Index Terms*—Empirical mode decomposition (EMD), image watermarking, multiband wavelets transformation (MWT).**

I. Introduction

With the rapid development of internet and wireless networks, multimedia security and digital rights management (DRM) are becoming increasingly important issues [1], [2]. The watermarking system has been viewed as a possible solution to control unauthorized duplication and redistribution of those multimedia data [2]–[5]. Robustness, perceptually invisibility, and security are the basic requirements for a robust watermarking system [6]. Seeking new watermark embedding strategy to achieve performance is a very challenging problem [6]. In this paper, we propose a new blind image watermarking scheme, which is based on the multiband wavelet transform [7], [8] and the empirical mode decomposition [9].

The watermark bits can be embedded either in the spatial domain or in the transform domain, while the latter watermark embedding strategy has been demonstrated to be more robust against most of attacks [3]. We take that latter watermarking embedding strategy in our image watermark embedding scheme, particularly we embed watermark bits indirectly in the multiband wavelet domain with the dilation factor $M \geq 2$ (see, for instance, [8] and [10]–[21] for the theory and various applications of multiband wavelets). For $M = 2$, there are lots of watermarking schemes available. For instance, Prayoth *et al.* [22] introduced a semi-blind watermarking scheme based on the two-band multiwavelet transform, which is shown to be robust to most of common image compressions. Hsieh *et al.* [23] proposed a nonblind watermarking scheme based on the two-band wavelet transform and the qualified significant wavelet tree (QSWT), which is robust to JPEG compression, image cropping, median filter etc., Lahouari *et al.* [24] suggested a watermarking algorithm based on the balanced two-band multiwavelet transform and the well-established perceptual model, which is adaptive and highly robust. Ng *et al.* [25] put forward a maximum-likelihood detection scheme that is based on modelling the distribution of the image DWT coefficients using a Laplacian probability distribution function (PDF). In [26], Bao *et al.* proposed a watermarking scheme by using a quantization-index-modulation (QIM) process via wavelet domain singular value decomposition (SVD). That scheme is robust against JPEG compression but extremely sensitive to filtering and random noising. In this paper, we use the multiband wavelet domain, instead of the two-band wavelet domain, to embed the watermark bits for the reason that the multiband wavelet domain provides more capacity for watermarking (see Section IV), and more flexible tiling of the scale-space plane. (see Fig. 1). Particularly, applying the MWT with the dilation factor $M > 2$ an image is decomposed into M^2 subimages with narrower frequency bandwidth in different scales and directions. The $(M-2)^2$ subimages thus generated with middle frequency are favorable blocks to embed watermark bits in our watermark embedding strategy due to the robustness against JPEG compression and various noise attacks.

For the robustness of an image watermarking system, the watermark bits are usually embedded in the perceptually significant components, mostly the low or middle frequency components of the image [3]. The EMD, first proposed in [9] and later demonstrated to be very useful in many areas [27]–[30], provides a self-adaptive decomposition of a signal, and the mean trend, the coarsest component, of the signal is highly robust

Manuscript received July 29, 2006; revised April 24, 2007. N. Bi, D. Huang, and J. Huang were supported in part by the NSFC (10631080, 10471123, 60475042, 60325208, 90604008, 60633030), in part by the NSF of Guangdong (04205407, 5300620), and in part by the 973 Program (2006CB303104). The associate editor coordinating the review of this manuscript and approving it for publication was Dr. Dimitri Van De Ville.

N. Bi is with the Department of Scientific Computing and Computer Applications and the Guangdong Key Laboratory of Information Security Technology, Sun Yat-Sen University, Guangzhou 510275, China (e-mail: mcsbn@mail.sysu.edu.cn).

Q. Sun is with the Department of Mathematics, University of Central Florida, Orlando, FL 32816 USA (e-mail: qsun@mail.ucf.edu).

D. Huang is with the Department of Scientific Computing and Computer Applications, Sun Yat-Sen University, Guangzhou 510275, China (e-mail: hdren@mail.sysu.edu.cn).

Z. Yang is with the Information Science School, GuangDong University of Business Studies, Guangzhou 510320, China (e-mail: yangyangzh@tom.com).

J. Huang is with the School of Information Science and Technology and the Guangdong Key Laboratory of Information Security Technology, Sun Yat-Sen University, Guangzhou 510275, China (e-mail: isshjw@mail.sysu.edu.cn).

Color versions of one or more of the figures in this paper are available online at http://ieeexplore.ieee.org.

Digital Object Identifier 10.1109/TIP.2007.901206

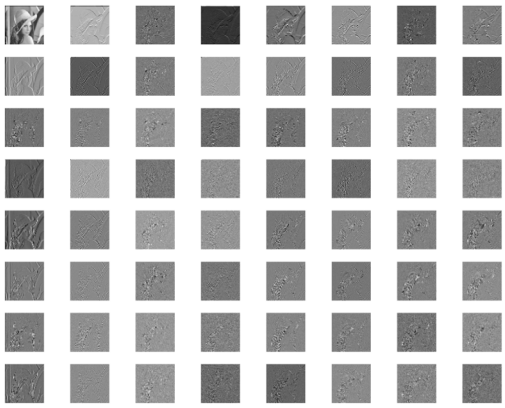

Fig. 1. Eight-band discrete wavelet decomposition of the "Lena" image.

under noise attack and JPEG compression. So, we select the mean trend of each subimage in the multiband wavelet domain, instead of the subimage itself, to embed the watermark bits. Our experimental results show that the watermarking based on the MWT and EMD is robust against JPEG compression, Gaussian noise, Salt and Pepper noise, median filtering and ConvFilter (Gaussian filtering and sharpening) attacks.

The rest of this paper is organized as follows. We first give an overview of MWT and EMD in Section II. The new blind watermarking scheme based on the MWT and EMD is proposed in Sections III and IV. The experimental results of our watermarking scheme and the comparison with the other watermarking schemes are given in Section V. The conclusions of this paper are stated in Section VI.

II. Multiband Wavelet Transformation and Empirical Mode Decomposition

In this section, we give an overview of Mallat's multiband discrete wavelet transform (MWT) for images [7], [8], [31], and the empirical mode decomposition (EMD) for 1-D signals [9].

A. Multiband Discrete Wavelet Decomposition and Reconstruction Algorithm

Given a dilation factor $M \geq 2$, the 1-D filters $H_0(\xi) = \sum_{n\in\mathbb{Z}} g_0(n)e^{-in\xi}$ and $H_l(\xi) = \sum_{n\in\mathbb{Z}} g_l(n)e^{-in\xi}, 1 \leq l \leq M-1$, are said to be *scaling filter* and *wavelet filters*, respectively, if

$$H_l(0) = \delta_{l0}$$

and

$$\sum_{m=0}^{M-1} H_l\left(\xi + \frac{2m\pi}{M}\right)\overline{H_{l'}\left(\xi + \frac{2m\pi}{M}\right)} = \delta_{ll'}$$

for all $0 \leq l, l' \leq M-1$, where $\delta_{ll'} = 1$ if $0 \leq l = l' \leq M-1$, and 0 otherwise ([7], [8], [31]). Clearly, a scaling filter H_0 is a low-pass filter, while wavelet filters $H_l, 1 \leq l \leq M-1$, are high-pass filters.

Given 1-D scaling filter $H_0(\xi)$ and wavelet filters $H_l(\xi), 1 \leq l \leq M-1$, using tensor product method one constructs a family of 2-D scaling filter

$$H_{00}(\xi,\eta) := H_0(\xi)H_0(\eta)$$

TABLE I
Impulse Responses of the Four-Tap Two-Band Wavelet Transform

n	$g_0(n)$	$g_1(n)$
0	λ_1	λ_3
1	λ_2	-λ_4
2	λ_4	λ_2
3	λ_3	-λ_1

and wavelet filters

$$H_{kl}(\xi,\eta) := H_k(\xi)H_l(\eta)$$

with $0 \leq k, l \leq M-1$ and $(k,l) \neq (0,0)$. For the above 2-D scaling filter $H_{00}(\xi,\eta)$ and wavelet filters $H_{kl}(\xi,\eta), 0 \leq k, l \leq M-1$ with $(k,l) \neq (0,0)$, we may use Mallat's multiband discrete wavelet decomposition algorithm to decompose an image $C, C = (c(m,n))$, into M^2 subimages $C_{kl} = (c_{kl}(m,n))$ in the wavelet domain

$$c_{kl}(m,n) = \sum_{m',n'\in\mathbb{Z}} c(m',n')g_{kl}(m'-Mm, n'-Mn)$$

where

$$H_{kl}(\xi,\eta) = \sum_{m,n\in\mathbb{Z}} g_{kl}(m,n)e^{-i(m\xi+n\eta)}, 0 \leq k, l \leq M-1.$$

The subimages C_{00} and $C_{kl}, 1 \leq k, l \leq M-1$ are usually called the blurred and detailed components respectively in the wavelet domain. In Fig. 1, we use Mallat's multiband discrete wavelet decomposition to decompose the image "Lena" into 64 subimages in the wavelet domain, where the 1-D scaling and wavelet filters are chosen from Table III with dilation $M = 8$ and the parameter λ is given in Table IV.

Given 2-D scaling filter $H_{00}(\xi,\eta)$ and wavelet filters $H_{kl}(\xi,\eta), 0 \leq k, l \leq M-1$, with $(k,l) \neq (0,0)$, we may use Mallat's multiband discrete wavelet reconstruction algorithm associated with the above 2-D scaling filter and wavelet filters to reconstruct the original image $C = (c(m,n))$ from M^2 subimages $C_{kl} = (c_{kl}(m,n))$ in the wavelet domain

$$c(m,n) = \frac{1}{M^2}\sum_{k,l=0}^{M-1}\sum_{m',n'\in\mathbb{Z}} c_{kl}(m',n')g_{kl}(m-Mm', n-Mn').$$

The reader may refer to [7], [8], and [31] and references therein for more information about multiband wavelet decomposition and reconstruction of an image.

For $\lambda \in [0, 2\pi]$, we set $\lambda_1 = (1+\sqrt{2}\cos\lambda)/4, \lambda_2 = (1-\sqrt{2}\sin\lambda)/4, \lambda_3 = (1+\sqrt{2}\sin\lambda)/4$, and $\lambda_4 = (1-\sqrt{2}\cos\lambda)/4$. In this paper, we will use the following parameterized multiband scaling and wavelet filters, where M is the dilation and λ is the parameter.

- $M = 2$, and the impulse response of the scaling filter $H_0(\xi) = \sum_{n=0}^{3} g_0(n)e^{-in\xi}$ and wavelet filter $H_1(\xi) = \sum_{n=0}^{3} g_1(n)e^{-in\xi}$ are listed in Table I. The above scaling and wavelet filter become the Daubechies' scaling and wavelet filters in [32] if $5\pi/12$ is chosen as the parameter λ, and the Haar scaling and wavelet filters if we let $\lambda = 5\pi/4$.

TABLE II
IMPULSE RESPONSES OF THE EIGHT-TAP FOUR-BAND WAVELET TRANSFORM

n	$g_0(n)$	$g_1(n)$	$g_2(n)$	$g_3(n)$
0	λ_1	-λ_2	-λ_2	λ_1
1	λ_2	-λ_1	λ_1	-λ_2
2	λ_3	λ_4	λ_4	λ_3
3	λ_4	λ_3	-λ_3	-λ_4
4	λ_4	-λ_3	-λ_3	λ_4
5	λ_3	-λ_4	λ_4	-λ_3
6	λ_2	λ_1	λ_1	λ_2
7	λ_1	λ_2	-λ_2	-λ_1

TABLE III
IMPULSE RESPONSES OF THE SIXTEEN-TAP EIGHT-BAND WAVELET TRANSFORM

n	g_0	g_1	g_2	g_3	g_4	g_5	g_6	g_7
0	λ_2	-λ_2	λ_1	-λ_1	-λ_1	λ_1	-λ_2	λ_2
1	λ_1	-λ_1	λ_2	-λ_2	λ_2	-λ_2	λ_1	-λ_1
2	λ_1	-λ_1	-λ_2	λ_2	λ_2	-λ_2	-λ_1	λ_1
3	λ_2	-λ_2	-λ_1	λ_1	-λ_1	λ_1	λ_2	-λ_2
4	λ_3	-λ_3	λ_4	-λ_4	-λ_4	λ_4	-λ_3	λ_3
5	λ_4	-λ_4	λ_3	-λ_3	λ_3	-λ_3	λ_4	-λ_4
6	λ_4	-λ_4	-λ_3	λ_3	λ_3	-λ_3	-λ_4	λ_4
7	λ_3	-λ_3	-λ_4	λ_4	-λ_4	λ_4	λ_3	-λ_3
8	λ_3	λ_3	-λ_4	-λ_4	-λ_4	-λ_4	λ_3	λ_3
9	λ_4	λ_4	-λ_3	-λ_3	λ_3	λ_3	-λ_4	-λ_4
10	λ_4	λ_4	λ_3	λ_3	λ_3	λ_3	λ_4	λ_4
11	λ_3	λ_3	λ_4	λ_4	-λ_4	-λ_4	-λ_3	-λ_3
12	λ_2	λ_2	-λ_1	-λ_1	-λ_1	-λ_1	λ_2	λ_2
13	λ_1	λ_1	-λ_2	-λ_2	λ_2	λ_2	-λ_1	-λ_1
14	λ_1	λ_1	λ_2	λ_2	λ_2	λ_2	λ_1	λ_1
15	λ_2	λ_2	λ_1	λ_1	-λ_1	-λ_1	-λ_2	-λ_2

- $M = 4$, and the impulse responses of the symmetric scaling filter $H_0(\xi) = \sum_{n=0}^{7} g_0(n)e^{-in\xi}$ and (anti)symmetric wavelet filters $H_l(\xi) = \sum_{n=0}^{7} g_l(n)e^{-in\xi}, 1 \le l \le 3$ are shown in Table II. The scaling and wavelet filters are introduced in [33].
- $M = 8$, and the impulse response of scaling and wavelet filters are given in Table III. One may verify that the above new one-parameter scaling and wavelet filters have minimal numbers of nonzero taps in the class of (anti)symmetric scaling and wavelet filters with dilation $M = 8$ except the Haar scaling and wavelet filters, which is the special case of $\lambda = 3\pi/4$.

B. Empirical Mode Decomposition

An *intrinsic mode function* (IMF) is a function that satisfies two conditions: 1) in the whole data set, the number of extrema and the number of zero crossing must either equal or differ at most by one; and 2) at any point, the mean value of envelope defined by the local maxima and the envelope defined by the local minima is zero [9]. An algorithm, known as the EMD to decompose a signal into finitely many IMFs and a mean trend, is proposed in [9] (see [27]–[30] for various applications of the EMD to gearbox fault diagnosis, image analysis, neural data analysis, and the fault diagnosis of roller bearings).

The EMD, which extracts all IMFs from a signal $r_0(t)$, can be described as follows [9].

Step 1) The first component $c_1(t)$ for the signal $r_0(t)$.
- a) Identify all the local extrema of the signal $r_0(t)$.
- b) Connect all the local maxima by a cubic spline line as the upper envelope; and all the local minima by a cubic spline line as the lower envelope (Remark: The upper and lower envelopes should cover all the data between them).
- c) The mean of upper and low envelope value is designated as $m_{10}(t)$, and the difference between the signal $r_0(t)$ and $m_{10}(t)$ is denoted by $h_{10}(t) = r_0(t) - m_{10}(t)$.
- d) If $h_{10}(t)$ is not an IMF, we replace the signal $r_0(t)$ by $h_{10}(t)$ and repeat the above procedure [Steps 1a)–1c)] for $h_{10}(t)$.
- e) The sifting process stops until the resulting difference between the mean of upper and low envelope value in Step 1c) and the initial signal in Step 1a) is an IMF. Then we let the resulting IMF be the first component $c_1(t)$ of the original signal $r_0(t)$ [the first IMF component $c_1(t)$ is obtained from the original data, and contains the finest scale (or the shortest period component) of the signal $r_0(t)$, as shown in Fig. 2].

Step 2) Let $r_1(t) = r_0(t) - c_1(t)$. If $r_1(t)$ becomes a monotonic function from which no more IMFs can be extracted, then we stop the decomposition process. Otherwise, replace $r_0(t)$ by $r_1(t)$ and repeat Step 1) to find the first component for $r_1(t)$.

Given a signal $r_0(t)$, applying the above algorithm we obtain a family of signals $c_k(t)$ and $r_k(t), 1 \le k \le n$, such that $c_k(t)$ is the first component of the signal $r_{k-1}(t)$, and $r_k(t) = r_{k-1}(t) - c_k(t)$ for $1 \le k \le n$, and r_n does not have any IMFs

TABLE IV
THE OPTIMAL PARAMETER λ_{opt} FOR WHICH $P_{I,M}(\lambda)$ TAKES THE MINIMAL VALUE

Dilation	Lena	Baboon	Peppers	Goldhill
M=8	2.58	2.61	2.51	2.58
M=4	2.70	2.76	2.70	2.73
M=2	2.89	2.86	2.95	2.92

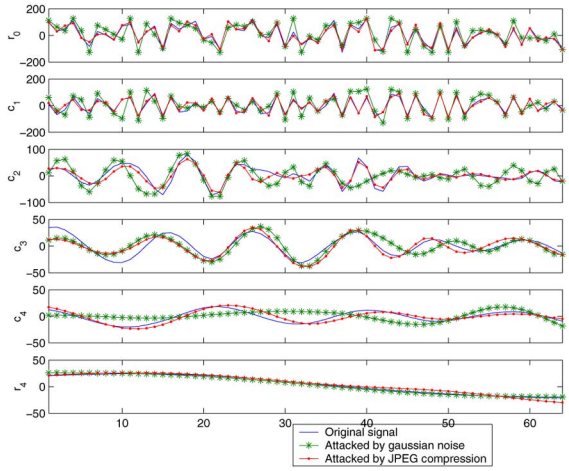

Fig. 2. Original and the attacked signals r_0, and its IMFs c_1, c_2, c_3, c_4 and mean trend r_4 obtained via the EMD.

to be extracted from. This leads to the following empirical mode decomposition of the original signal $r_0(t)$

$$r_0(t) = \sum_{j=1}^{n} c_j(t) + r_n(t). \tag{1}$$

In brief, the EMD extracts the finest scale or the shortest period component from the signal step by step, and the remainder of the sifting process, to be named as the *mean trend*, is the coarsest component of the signal (see Fig. 2). Clearly, no IMF can be extracted from the mean trend of a signal. Moreover, our simulation shows that the mean trend is extremely stable for Gaussian noise and JPEG compression attack (see Fig. 2). This *new* observation is the motivation that we select the EMD, and embed the watermark bits into the mean trend of the subimages in the multiband wavelet domain, instead of the subimages directly as in most of the literature.

III. Watermark Embedding and Detecting

In this section, we propose a novel watermark embedding and detecting algorithm based on the MWT and EMD.

A. Watermark Embedding

For an image I of size $N_1 \times N_2$, we use the following steps to embed the watermark in the image.

Multiband Discrete Wavelet Decomposition: Select a dilation factor $M \geq 2$, and 1-D scaling and wavelet filters $H_l(\xi), 0 \leq l \leq M-1$. Via tensor product, we generate 2-D scaling filter $H_{00}(\xi,\eta) := H_0(\xi)H_0(\eta)$ and wavelet filters $H_{ll'}(\xi,\eta) = H_l(\xi)H_{l'}(\eta)$, where $0 \leq l,l' \leq M-1$ but $(l,l') \neq (0,0)$. Applying the 2-D Mallat's discrete wavelet decomposition algorithm with the above scaling and wavelet filters, we decompose the image I into M^2 subimages $I_{ll'}, 0 \leq l,l' \leq M-1$. In particular, the subimages $I_{ll'}, 0 \leq l,l' \leq M-1$, of sizes $N_1/M \times N_2/M$ are obtained by M-subsampling the convolution between the original image I and the scaling (wavelet) filters $H_{ll'}$. In our simulation, the dilation M is chosen from $\{2,4,8\}$, and the coefficients of filters are taken from Tables I–III.

Watermark Embedding Domain: Applying Mallat's discrete multiband wavelet decomposition algorithm *once* in our watermarking process when the dilation $M = 4, 8$, or *twice or more* for the wavelet decomposition with dilation $M = 2$ [22]–[24], we obtain a wavelet decomposition of the original image with enough resolution and enough subimages. To find suitable subimages to embed watermark bits, we divide subimages in the multiband wavelet domain into three classes: $\mathcal{L}_F = \{H_{kl}, kl = 0\}, \mathcal{M}_F = \{H_{kl}, 1 \leq k,l \leq M-2\}$ and $\mathcal{H}_F = \{H_{kl}, (k-M+1)(l-M+1) = 0, kl \neq 0\}$. The subimages in the subband $\mathcal{L}_F$ include an approximation of the original image, and then embedding watermarks in those subimages may easily result in visual block effects. On the other hand, the subimages in the subband $\mathcal{H}_F$ is considered as components with highest frequency, and then the watermark may not be detected if the watermark is embedded into those subimages and the watermarked subimages are attacked by postprocessing such as JPEG compression. So, in our watermarking scheme, we select subimages in the subband $\mathcal{M}_F$ as our favorable blocks to embed watermark bits in our watermarking scheme. Consequently, it is demonstrated that this watermark embedding strategy results in better robustness against JPEG compression and visual perception. Moreover, applying the MWT with dilation M decomposes an image into M^2 subimages with $(M-2)^2$ subimages having subband $\mathcal{M}_F$, and, hence, selecting a higher dilation factor M and appropriate filters may help us to improve the performance of our watermark process (see Section V for the experimental confirmation of that observation).

Empirical Mode Decomposition: For the subimages $I_{ll'}, 1 \leq l,l' \leq M-2$, we divide each of them into $K \times K$ nonoverlapped subblocks $I_{ll';kk'}, 1 \leq k,k' \leq K$, then convert each subblock into a 1-D signal, which is still denoted by $I_{ll';kk'}$. Now we apply the EMD to each of these time signals $I_{ll';kk'}$

$$I_{ll'kk'} = \sum_{j=1}^{n_{ll';kk'}} c_j(I_{ll';kk'}) + r_{n_{ll';kk'}}(I_{ll';kk'}) \tag{2}$$

and store the mean trend $r_{n_{ll';kk'}}(I_{ll';kk'}), 1 \leq l,l' \leq M-2, 1 \leq k,k' \leq K$.

Our simulation shows that our watermarking scheme based on MWT and EMD has better performance in efficiency, accuracy, and robustness if the size of each subblock is around 8×8. So in the simulation, we may select the constant K so that each subblock is of size 8×8. For instance, we let $K = 8$ if the image is of size $512 \times$ and the dilation M of the multiband wavelet transform is 8.

Watermark Embedding: Given a watermark $W = \{b_i = \pm 1 : 1 \leq i \leq m,\}$, let $\mathcal{A}$ be a one-to-one mapping from $\{1,\ldots,m\}$ to $\{1,\ldots,M-2\}^2 \times \{1,\ldots,K\}^2$ [see the formula (5) in our simulation] and embed the watermark bit $b_i, 1 \leq i \leq m$, into the subblock $I_{\mathcal{A}(i)}$ by changing its mean trend $r_{n_{\mathcal{A}(i)}}(I_{\mathcal{A}(i)})$ with another mean trend $r^*_{n_{\mathcal{A}(i)}}(I_{\mathcal{A}(i)})$ [see the formula (6) in our simulation]. The new subblocks $I^*_{ll';kk'}, 1 \leq l,l' \leq M-2, 1 \leq k,k' \leq K$, after embedding watermark bit stream $\{b_1,\ldots,b_m\}$, are given by the following equations:

$$\begin{aligned} I^*_{ll';kk'} &= I_{ll';kk'} - r_{n_{\mathcal{A}(i)}}(I_{\mathcal{A}(i)}) + r^*_{n_{\mathcal{A}(i)}}(I_{\mathcal{A}(i)}) \\ &= \sum_{j=1}^{n_{ll';kk'}} c_j(I_{ll';kk'}) + r^*_{n_{ll';kk'}}(I_{ll';kk'}) \end{aligned} \tag{3}$$

if $(l,l',k,k') \in \mathcal{A}\{1,\ldots,m\}$ and

$$I^*_{ll';kk'} = I_{ll';kk'} \tag{4}$$

if $(l,l',k,k') \notin \mathcal{A}\{1,\ldots,m\}$.

In our simulation, we use the following one-to-one mapping $\mathcal{A}$

$$\begin{aligned} \mathcal{A} : \{1,\ldots,m\} \ni i \longmapsto \mathcal{A}(i) := (l,l',k,k') \in \\ \{1,\cdots,M-2\}^2 \times \{1,\cdots,K\}^2 \end{aligned} \tag{5}$$

where l,l',k,k' are determined by the unique decomposition $i-1 = (K-k') + (K-k)K + (M-2-l')K^2 + (M-2-l)(M-2)K^2, 1 \leq i \leq m$. From the definition of the above

map, we see that the capacity of our watermarking process and the length m of the watermark bit should satisfy the inequality

$$m \le (M-2)^2 K^2.$$

In our simulation, we write the watermarked subblock $I^*_{\mathcal{A}(i)}$, which is obtained by embedding the watermark bits b_i into the subblock $I_{\mathcal{A}(i)}$, as follows:

$$I^*_{\mathcal{A}(i)} = I_{\mathcal{A}(i)} - r_{\mathcal{A}(i)} + r^*_{\mathcal{A}(i)}$$

where $r_{\mathcal{A}(i)}$ is the mean tread of the subblock $I_{\mathcal{A}(i)}, r^*_{\mathcal{A}(i)}$ is defined by

$$r^*_{\mathcal{A}(i)}(t) = \begin{cases} \rho(r_{\mathcal{A}(i)}(t) - \min_\xi(r_{\mathcal{A}(i)}(\xi))) \\ \quad + \max(S, \min_\xi(r_{\mathcal{A}(i)}(\xi))), & \text{if} \quad b_i = 1 \\ \rho(r_{\mathcal{A}(i)}(t) - \max_\xi(r_{\mathcal{A}(i)}(\xi))) \\ \quad + \min(-S, \max_\xi(r_{\mathcal{A}(i)}(\xi))), & \text{if} \quad b_i = -1 \end{cases} \tag{6}$$

ρ and $S \ge 0$ are watermark strengths to be determined in the next section.

Watermarked Image: For any $1 \le l, l' \le M-1$, we combine the watermarked blocks $I^*_{ll';kk'}, 1 \le k, k' \le K$, into a subimage $I^*_{ll'}$ in a reverse way to split a subimage into subblocks with the formula (3) or (4). Defining $I^*_{ll'} = I_{ll'}$ for those $l, l' \in \{0, 1, \ldots, M-1\}$ satisfying $ll' = 0$, we then obtain M^2 subimages $I^*_{ll'}, 0 \le l, l' \le M-1$, of size $N_1/M \times N_2/M$. Applying Mallat's multiband discrete wavelet reconstruction to those M^2 images $I^*_{ll'}, 0 \le l, l' \le M-1$, leads to the watermarked image I^* of size $N_1 \times N_2$.

B. Watermark Detection

Given a test image I^*, we extract the watermark as follows.

i) Apply multiband discrete wavelet decomposition with the same scaling and wavelet filters as in the embedding process to the image I^*. We then obtain M^2 subimages $I^*_{ll'}, 0 \le l, l' \le M-1$, in the wavelet domain.

ii) Split each subimage $I^*_{ll'}$ into K^2 subblocks $I^*_{ll';kk'}, 1 \le k, k' \le K$, where $1 \le l, l' \le M-2$.

iii) Take the same one-to-one map $\mathcal{A}$ as the one in the watermark embedding process.

iv) For any $1 \le i \le m$, consider $I^*_{\mathcal{A}(i)}$ as a 1-D signal and apply the EMD to it

$$I^*_{\mathcal{A}(i)} = \sum_{j=1}^{n_{\mathcal{A}(i)}} c_j + r_{n_{\mathcal{A}(i)}}(I^*_{\mathcal{A}(i)})$$

where $c_j, 1 \le j \le n_{\mathcal{A}(i)}$, are IMFs and $r_{n_{\mathcal{A}(i)}}(I^*_{\mathcal{A}(i)})$ is the mean trend of $I^*_{\mathcal{A}(i)}$.

v) Use the mean trend $r_{n_{\mathcal{A}(i)}}(I^*_{\mathcal{A}(i)})$ to determine embedded bit b_i in $I^*_{\mathcal{A}(i)}$. In particular, we retrieve the watermark bit b_i from the watermarked block $I^*_{\mathcal{A}(i)}$ as follows:

$$\begin{cases} b = 1, & \text{if} \quad \sum_t r^*_{\mathcal{A}(i)}(t) > 0 \\ b = -1, & \text{if} \quad \sum_t r^*_{\mathcal{A}(i)}(t) \le 0 \end{cases} \tag{7}$$

where $r^*_{\mathcal{A}(i)}$ is the mean trend of the subblock $I^*_{\mathcal{A}(i)}$.

vi) Obtain the watermark bits $W = \{b_1, \ldots, b_m\}$.

Fig. 3. Original images Lena, Baboon, Peppers, and Goldhill of $512 \times 512 \times 8$ bits.

If the watermarking strength parameters ρ and S satisfy $\rho = 1$ and $S > 0$, one may verify from the procedure of the EMD that the mean trend of a watermarked subblock $I^*_{\mathcal{A}(i)}$ is same as the function $r^*_{\mathcal{A}(i)}(t)$ given in (6). Theoretically the watermark bits $b = 1$ or $b = -1$ can always be extracted by the algorithm (7) in this case. If the watermarking strength parameter $\rho \ne 1$ and $S = S(\rho, I)$ in the (9), our simulation shows that for the test images "Lena," "Baboon," "Peppers," and "Goldhill" of $512 \times 512 \times 8$ bits, no wrong watermark bit is detected by using (7). However, if $\rho \ne 1$ and $S \le S(\rho, I)$ in the (9) (for instance, S is sufficiently small), wrong watermarks bit may be detected for the test images.

IV. Optimization of The Parameters

In the previous section, we have presented our watermark embedding and detecting algorithms. The purpose of this section is then to consider the following problems: 1) how to determine the parameter λ in the scaling and wavelet filters; 2) how to adjust the watermark strength S and ρ in the watermark embedding process. In the following simulation, we will use the character string watermark "*SYS Univ*," and the test images "Lena," "Baboon," "Peppers," and "Goldhill" of $512 \times 512 \times 8$ bits, as shown in Fig. 3.

A. Scaling and Wavelet Filters in MWT

In the simulation, we use the parameterized impulse response in Tables I–III as the scaling and wavelet filters $H_l(\xi), 0 \le l \le M-1$, in our MWT. We define the percentage of energy with middle and high frequency by

$$P_{I,M}(\lambda) := \frac{E^\lambda_H(I)}{E(I)}$$

where $E(I) = (\sum_{i=1}^{N_1} \sum_{j=1}^{N_2} |I(i,j)|^2)^{1/2}$ is the total energy of the image $I, E^\lambda_H(I) = (\sum_{l,l'=1}^{M-1} |E(I_{ll'})|^2)^{1/2}$ is the total energy of subimages with middle and high frequency in the wavelet domain, and $I_{ll'}$ is the subimage associated with the wavelet filter $H_l(\xi)H_{l'}(\eta), 1 \le l, l' \le M-1$. The behavior of

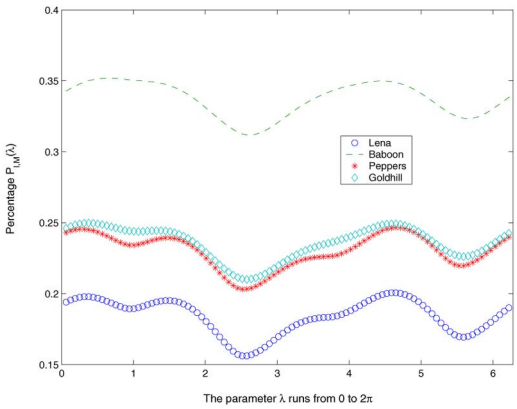

Fig. 4. $P_{I,M}(\lambda)$: The percentage of energy with middle and high frequencies in the wavelet domain for the Lena, Baboon, Peppers, and Goldhill images, where we use dilation factor 8 and wavelet filters in Table III.

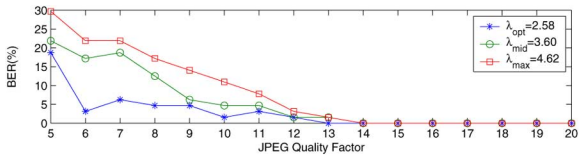

Fig. 5. BER of the extracted watermark from the watermarked "Lena" image under the attack of JPEG compression with JPEG factor from 5 to 20. In this simulation, we use 8 as the dilation factor, the filters in Table III as the filters in the MWT, and Lena image as the test image. The parameters $\lambda_{\rm opt}, \lambda_{\max}$ and $\lambda_{\rm mid}$ are so chosen that $P_{I,M}(\lambda_{\rm opt}) = \min_{0\le\lambda\le 2\pi} P_{I,M}(\lambda), P_{I,M}(\lambda_{\max}) = \max_{0\le\lambda\le 2\pi} P_{I,M}(\lambda)$ and $P_{I,M}(\lambda_{\rm mid}) = 1/2(P_{I,M}(\lambda_{\rm opt}) + P_{I,M}(\lambda_{\max}))$.

TABLE V
BER PERCENTAGE OF EXTRACTED WATERMARK BY APPLYING OUR MWT AND EMD ALGORITHM TO THE LENA IMAGE UNDER THE ATTACK OF JPEG COMPRESSION WITH JPEG COMPRESSION QUALITY FACTOR Q RUNNING FROM 2 TO 20, THE STRENGTH PARAMETER $\rho = 0, 0.4, 1, 2$, AND THE WATERMARKING STRENGTH $S := S(\rho, I)$ IS DEFINED AS IN (9)

Q	2	4	6	8	10	14	18	20
$\rho = 0, S = 65$	21.88	14.06	1.56	1.56	0	0	0	0
$\rho = 0.4, S = 63$	23.44	14.06	3.13	1.56	0	0	0	0
$\rho = 1, S = 58$	25.00	15.63	3.13	1.56	0	0	0	0
$\rho = 2, S = 51$	25.00	21.88	4.69	3.13	0	0	0	0

the energy percentage for the Lena, Baboon, Peppers, and Goldhill images is shown in Fig. 4.

As our watermark is embedded in the multiband wavelets domain $\mathcal{M}_F$ and $\mathcal{H}_F$, the lesser energy of those subimages the lesser influence of the watermark process to the image. This also implies that larger watermark strength S can be added, and the corresponding watermarking algorithm could be more robust against various attacks. Based on the above ideas, we select the parameter λ so that $P_{I,M}(\lambda)$ takes the minimal value. In other words, the optimal parameter $\lambda_{\rm opt}$ for our watermarking scheme based on the MWT and EMD is the one that satisfies

$$P_{I,M}(\lambda_{\rm opt}) = \inf_{\delta\in[0,2\pi]} P_{I,M}(\delta) \tag{8}$$

(refer to Table IV for the optimal parameter $\lambda_{\rm opt}$ of the test images). Our experimental results indicate that our watermark embedding and detecting algorithms with optimal parameter $\lambda_{\rm opt}$ has minimal bit error rate (BER) under the attack of JPEG compression, as shown in Fig. 5.

Fig. 6. Watermarked "Lena," "Baboon," "Peppers," and "Goldhill" images with the watermarking strength parameters $\rho(I)$ and $S(I)$ in (10).

TABLE VI
FOR THE LENA IMAGE I, THE MAXIMAL WATERMARKING STRENGTH $S(\rho, I)$ DECREASES FROM 65 TO 51 WHEN THE PARAMETER ρ RUNS FROM 0 TO 2

ρ	0.0	0.2	0.4	0.6	0.8	1.0	1.2	1.4	1.6	1.8	2.0
S	65	64	63	61	60	58	57	55	54	52	51

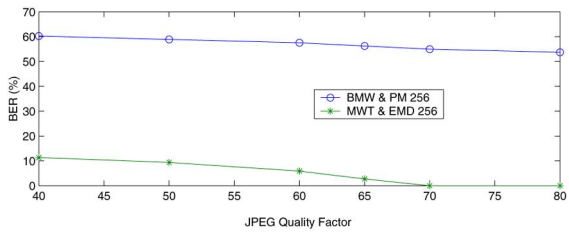

Fig. 7. BERs to extract watermarks using our watermark embedding and detecting method (MWT and EMD) and the balanced two-band multiwavelet transform and the well-established perceptual model (BMW and PM) in the presence of JPEG compression with JPEG quality factor from 40 to 80.

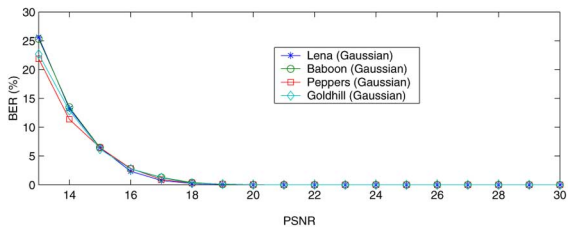

Fig. 8. Mean value of BER of the extracted watermark under Gaussian noise attack for 10 000 tests.

We may use other optimization to select the parameter λ in the MWT. For instance, we may replace the percentage $P_{I,M}(\lambda)$ of energy with high frequency by the distance $d_\lambda = (\int_{\pi/8}^{\pi} |H_0(\xi)|^2 d\xi)^{1/2}$ between the ideal low-pass filter and the low-pass filter $H_0(\xi)$, which is independent of images. In this case, the quantity d_λ achieves its minimal value when λ takes $\lambda'_{\rm opt} = 2.5876$ for $M = 8, \lambda'_{\rm opt} = 2.7646$ for $M = 4$ and $\lambda'_{\rm opt} = 2.8903$ for $M = 2$, which are almost the same

TABLE VII
BER OF EXTRACTED WATERMARK BY OUR MWT AND EMD ALGORITHM

Image	Dilation M	Parameter λ_{opt}	PSNR	JPEG Compression, BER(%)						
				5	10	15	20	25	30	40
Lena	8	2.58	42.0 dB	6.25	0	0	0	0	0	0
	4	2.70	42.0 dB	40.63	29.69	20.31	10.94	3.13	0	0
	2	2.89	42.0 dB	42.19	17.19	6.25	4.69	1.56	0	0
	2 (Haar)	$5\pi/4$	42.0 dB	25.00	9.38	0	0	0	0	0
Baboon	8	2.61	42.0 dB	4.69	0	0	0	0	0	0
	4	2.76	42.0 dB	51.56	20.31	6.25	1.56	1.56	0	0
	2	2.86	42.0 dB	29.69	4.69	3.13	1.56	1.56	0	0
	2 (Haar)	$5\pi/4$	42.0 dB	10.94	0	0	0	0	0	0
Peppers	8	2.51	42.0 dB	6.25	0	0	0	0	0	0
	4	2.70	42.0 dB	42.19	28.13	14.06	6.25	0	0	0
	2	2.95	42.0 dB	39.06	14.06	7.81	1.56	1.56	0	0
	2 (Haar)	$5\pi/4$	42.0 dB	23.44	0	0	0	0	0	0
Goldhill	8	2.58	42.0 dB	10.94	0	0	0	0	0	0
	4	2.73	42.0 dB	37.50	29.69	20.31	7.81	3.13	0	0
	2	2.92	42.0 dB	34.38	12.50	6.25	4.69	0	0	0
	2 (Haar)	$5\pi/4$	42.0 dB	29.69	1.56	0	0	0	0	0

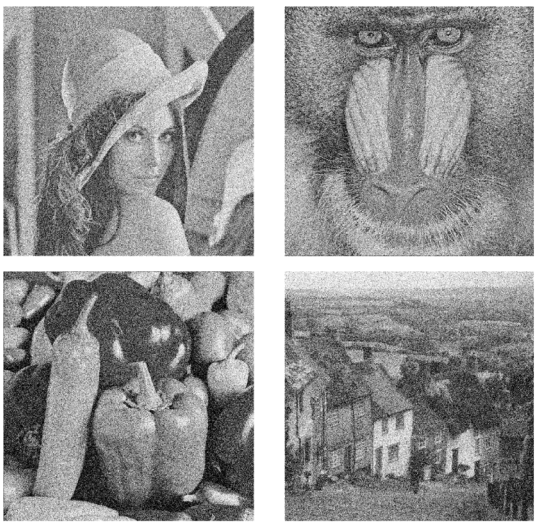

Fig. 9. Watermarked image under Gaussian noise attack with PSNR=20 dB.

TABLE VIII
COMPARISON BETWEEN OUR WATERMARKING METHOD (MWT AND EMD) AND THE MAXIMUM LIKELIHOOD DETECTION METHOD ON THE WAVELET DOMAIN (MLDM) IN [25]: PERCENTAGE OF SUCCESSFUL WATERMARK DETECTIONS (PSWD) UNDER JPEG COMPRESSION ATTACKS

Method	Image	PSNR	JPEG Compression, BER(%)				
			10	20	30	40	50
MLDM [25]	Lena	45 dB	-	-	-	-	8.59
MWT & EMD	Lena	45 dB	19.50	2.32	0.77	0	0
MLDM [25]	Peppers	45 dB	-	-	-	-	3.73
MWT & EMD	Peppers	45 dB	9.35	3.89	0	0	0

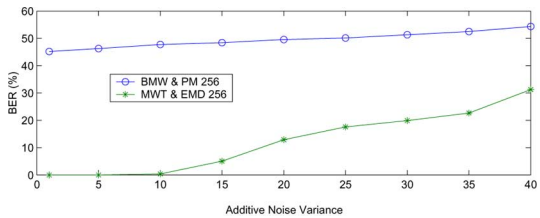

Fig. 10. BERs to extract watermarks using our watermark embedding and detecting method (MWT and EMD) and the balanced two-band multiwavelet transform and the well-established perceptual model (BMW and PM) in the presence of Gaussian noise attacks with additive noise variance from 1 to 40.

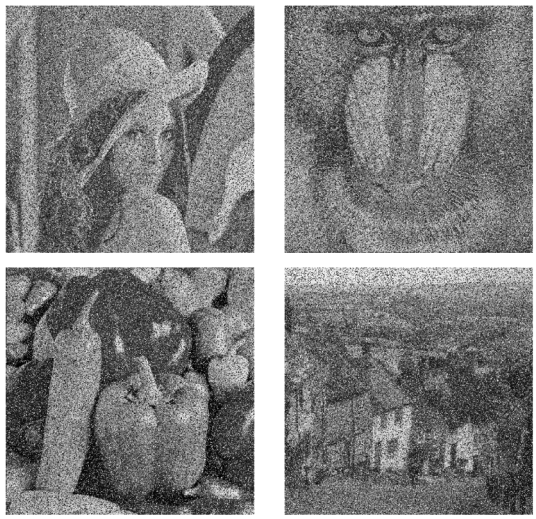

Fig. 11. Watermarked image with 30% Salt and Pepper noise attack.

as those listed in Table IV. So in some situations we may use the optimal parameter $\lambda'_{\rm opt}$ for the quantity d_λ, a parameter independent of images, as an almost-optimal substitution to the optimal parameter $\lambda_{\rm opt}$ in (8) for our watermark embedding and detecting scheme.

B. Watermark Strength

In the watermark embedding formula (6), there are two parameters ρ and S in our watermarking process. An immediate question is how to adjust those watermark strengths ρ and S such that our watermarking scheme have better performance? For the original image I, we denote by $I^*(\rho, S)$ the watermarked image obtained by 1) applying the wavelet decomposition algorithm with the filters in Tables I, II, or III, and the optimal parameter $\lambda_{\rm opt}$ determined by (8) to the original image I, 2) embedding the watermarking bits by (6), and 3) applying the wavelet reconstruction algorithm with the same filters and parameter as in the wavelet decomposition algorithm.

TABLE IX
MEAN VALUE OF BER OF EXTRACTED WATERMARK UNDER THE SALT AND PEPPER NOISE ATTACK FOR 10 000 TESTS, WHERE THE PERCENTAGE P OF THE SALT AND PEPPER NOISE ATTACK RUNS FROM 5 TO 30

	Lena		Baboon		Peppers		Goldhill	
P	PSNR	BER(%)	PSNR	BER(%)	PSNR	BER(%)	PSNR	BER(%)
5	24.58	0.00	24.69	0.00	24.16	0.00	24.35	0.00
10	21.62	0.00	21.72	0.01	21.19	0.00	21.38	0.04
15	19.87	0.06	19.97	0.07	19.44	0.09	19.64	0.11
20	18.62	0.30	18.73	0.47	18.20	0.39	18.39	0.58
25	17.66	0.73	17.76	1.27	17.24	1.02	17.43	1.23
30	16.87	1.95	16.98	2.62	16.45	2.20	16.64	2.05

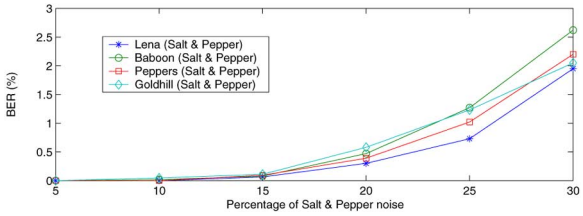

Fig. 12. Mean value curve of BER of the extracted watermark under Salt and Pepper noise attack for 10 000 tests.

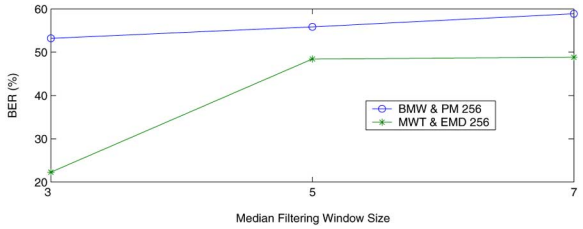

Fig. 13. BERs to extract watermarks using our watermark embedding and detecting method (MWT and EMD) and the balanced two-band multiwavelet transform and the well-established perceptual model (BMW and PM) in the presence of the median filtering attack with filter length 3, 5, and 7.

The PSNR is popularly used to measure the similarity between the original image and the watermarked image, while higher PSNR usually implies higher fidelity of the watermarked image. In most of our simulation, we select 42 dB as the balancing point of PSNR for enough visual imperceptibility and high robustness against various attacks. In the comparison with results [24] and [25] where watermark bits with different length are embedded in an image, we will use 38 and 45 dB as the balancing point of PSNR, respectively.

From the demonstration, we observe that 1) if we fix the watermarking parameter ρ, then bigger watermarking strength S results in higher robustness of our watermark process, while on the other hand the unreasonably big watermarking strength S may result in the watermark perceptually visible in the watermarked image; and 2) if we require the same PSNR for the watermarked image, then the strength parameter ρ has less significant influence than the watermarking strength S to the robustness of our watermark process; see Table V. So, for the perceptually invisibility of the watermark and the maximal robustness of our watermarking procedure, the watermarking strength parameter $S^*(I)$ and $\rho^*(I)$ for an image I can be chosen as follows:

$$\begin{cases} \rho^*(I) = \operatorname{argmax}_\rho S(\rho, I) \\ S^*(I) = S(\rho^*(I), I) \end{cases}$$

TABLE X
BER OF EXTRACTED WATERMARK UNDER MEDIAN FILTER ATTACKS

Median Filter	Image	PSNR (dB)	BER (%)
3×3	Lena	30.46	0
	Baboon	26.97	0
	Peppers	29.67	0
	Goldhill	29.74	0
5×5	Lena	30.79	9.38
	Baboon	26.75	12.50
	Peppers	30.02	7.81
	Goldhill	29.90	9.38
7×7	Lena	30.66	12.50
	Baboon	26.52	12.50
	Peppers	29.98	9.36
	Goldhill	29.62	9.38
9×9	Lena	30.41	51.56
	Baboon	26.35	78.13
	Peppers	29.73	51.56
	Goldhill	29.24	79.69

where

$$S(\rho, I) := \max\{S : \mathrm{PSNR}(I, \rho, S) \geq 42\}. \tag{9}$$

We observe that the watermarking strength $S(\rho, I)$ decreases when the parameter ρ increases, see Table VI for the experimental results. So in the simulation, the watermarking strength parameter $S(I)$ and $\rho(I)$ for an image I is chosen as follows:

$$\begin{cases} \rho(I) = 0 \\ S(I) = S(\rho(I), I). \end{cases} \tag{10}$$

In Fig. 6, we list the watermarked "Lena," "Baboon," "Peppers," and "Goldhill" images with optimal watermarking strength parameters $\rho(I)$ and $S(I)$ in (10).

V. EXPERIMENTAL RESULTS AND DISCUSSIONS

In this section, we discuss the robustness of our watermark scheme against JPEG compression, Gaussian noise, salt and pepper noise, median filtering, ConvFilter (Gaussian filtering and Sharpening), and RotationScale attacks. Some comparisons with the watermarking schemes in [24] and [25] are also presented.

A. Robustness Against JPEG Lossy Compression

A watermarking system should be robust against JPEG compression. In Table VII, we present the experimental results for our watermarking system, MWT & EMD for short, against JPEG compression, where 2, 4, 8 are chosen as the dilation M, and the optimal parameters λ_{opt} in Table IV or the parameter $5\pi/4$ associated with the Haar's filter are chosen as the parameters in the scaling and wavelet filters $H_l, 0 \leq l \leq M-1$. This confirms that the selection of the dilation M and the parameter

λ may improve the performance of watermarking scheme based on the MWT and EMD.

To compare our watermarking algorithm (MWT and EMD) with the watermarking scheme based on the balanced two-band multiwavelet transform and the well-established perceptual model (BMW and PM) in [24], we perform the simulation to embed same watermark with 256 bits (instead of "SYS Univ" with 64 bits in our demonstration simulation) and PSNR (38 dB) for the watermarked image (instead of 42 dB in our demonstration simulation) as in [24] into the "Lena" image [for that the watermarking strength $\rho(I)$ and $S(I)$ is given by $\rho(I) = 0$ and $S(I) = \max\{S : \mathrm{PSNR}(I, \rho, S) \geq 38\}$ instead of by (10) in our demonstration simulation], see Fig. 7 for the simulation results. Similarly to compare our watermarking algorithm (MWT and EMD) with the maximum-likelihood detection method on the wavelet domain (MLDM) in [25], we do the experiment to embed same watermark with 100 bits and PSNR (45 dB) for the watermarked image as in [25] into the "Lena" and "Peppers" images (for that the watermarking strength $\rho(I)$ and $S(I)$ is adjusted accordingly); see Table VIII for the experimental results. The above comparisons clearly demonstrated that our watermarking method has better performance than the ones in [24] and [25] against JPEG compression.

B. Robustness Against Gaussian Noise

The EMD extracts components with finest scale (or shortest period) from the signal one by one, and, hence, the remainder of the decomposition, the mean trend, is the coarsest component of the signal. Thus, the mean trend of a signal is robust against Gaussian noise with mean zero since it is sifted into the first few IMFs, and has little influence to the mean trend (see Fig. 2). This indicates that our watermarking algorithm based on the MWT and EMD is robust against Gaussian noise, which is confirmed by our experiments, as shown in Fig. 8. After Gaussian noise attack and the PSNR drop to 20 dB, the BER of extracted watermark are still zero, as shown in Fig. 9.

Compared with [24] (see Fig. 10), our watermark scheme is more robust against Gaussian noise attack.

Salt and pepper noise can be roughly thought as a signal with plenty of high frequency. Hence, our watermark embedding and detecting scheme should be robust against the salt and pepper noise because the mean trend obtained by the empirical mode decomposition is *extremely* stable under noise attack with high frequency. Our experimental results show that the proposed watermarking scheme has approximately zero BER of extracted watermark under 5% salt and pepper noise attack, and the BER of extracted watermark are still less than 3% after 30% salt and pepper noise, see Fig. 11 for the watermarked "Lena," "Baboon," "Peppers," and "Goldhill" images corrupted by 30% salt and pepper noise. The reader may refer to Fig. 12 and Table IX for detailed performance of our watermarking scheme against the salt and pepper noise attack.

C. Robustness Against Median Filtering

The median filtering technique, a widely-used image processing technique, provides some smoothing of the finer details with the major edges preserved [24]. Our experimental results show that the watermark embedding and detecting algorithm developed in this paper has zero BER to extract watermarks for 3×3 median filter attack (see Table X for details). Compared with the watermarking scheme in [24], our watermarking scheme has better performance against the median filtering attack (see Fig. 13).

TABLE XI
BER OF EXTRACTED WATERMARK UNDER THE CONVFILTER ATTACK

Test image	Lena	Baboon	Peppers	Goldhill
Gaussian filtering	3.13	0	1.56	6.25
Sharpening	0	0	0	0

Fig. 14. Watermarked images with the Gaussian filtering attack.

Fig. 15. Watermarked images with the Sharpening filtering attack.

D. Robustness Against ConvFilter Attack

Using *StirMark Benchmark 4*, we test our watermarking scheme against the ConvFilter attack with Gaussian filtering and Sharpening. The experimental results using our MWT and EMD algorithm are listed in the Table XI, and the corresponding attacked images are shown in Figs. 14 and 15.

TABLE XII
BER OF EXTRACTED WATERMARK UNDER ROTATIONSCALE ATTACK

Angles of rotation	-2°	-1°	-0.75°	-0.5°	-0.25°	0.25°	0.5°	0.75°	1°	2°
Lena	43.75	57.81	59.38	45.31	6.25	7.81	43.75	54.69	53.13	60.94
Baboon	56.25	54.69	57.81	43.75	7.81	7.81	45.31	56.25	53.13	43.75
Peppers	62.50	54.69	57.81	43.75	6.25	6.25	40.63	60.94	62.50	48.44
Goldhill	53.13	60.94	4.69	43.75	7.81	7.81	50.00	59.38	50.00	57.81

E. Feebleness Against Geometric Distortion Attack

It is challenging to design a robust blind watermarking and detecting scheme against various geometric distortion attacks. Due to the geometrical structure of our multiband wavelet decomposition, the watermarking scheme proposed in this paper has high BER percentage (and, hence, are feeble) under the geometric distortion attack such as rotating, bending, cropping and resizing; see Table XII for the experimental results under the Rotation Scale attack. We notice that there are plenty of watermarking algorithms such as in [34] and [35], which are robust against geometric distortion attacks. We are working on the problem how to improve the multiband wavelet decomposition of images, and then developing a new watermarking scheme based on wavelets and EMD that is robust also against most of geometric distortion attack.

VI. CONCLUSION

The multiband wavelet transform has long been successfully applied in many engineering areas, such as edge detection, texture segmentation, classification, and remote sensing [16]–[21]. The MWT with dilation M decomposes an image into M^2 subimages with narrow frequency bandwidth in different scales and directions, and generates about $(M-2)^2$ subimages with middle frequency. Those properties of MWT inspire us to use the subimages in the multiband wavelet domain to embed watermark bits. The empirical mode decomposition extracts the finest scale component from a signal step by step, and the mean trend is *extremely stable* under high frequency noise attack. Therefore, we embed the watermark into the mean trend of each subimage in the multiwavelet domain to achieve better performance. Taking the advantages of the multiband wavelet transform and the empirical mode decomposition, in this paper we develop a novel blind watermark embedding and detecting scheme based on the MWT and EMD. Our experiments show that the proposed scheme is robust against JPEG compression, Gaussian noise, salt and pepper noise, median filtering, and ConvFilter (Gaussian filtering and Sharpening), but the proposed scheme has high BER percentage under some geometric distortion attacks such as rotating, bending, cropping and resizing due to the geometric structure of the multiband wavelet decomposition of an image.

ACKNOWLEDGMENT

The authors would like to thank the anonymous reviewers for their helpful comments and suggestions which led to the improvement of the results and the presentation of this paper.

REFERENCES

[1] M. Lesk, "The good, the bad, and the ugly: What might change if we had good DRM," *IEEE Security Privacy Mag.*, vol. 1, no. 3, pp. 63–66, May/Jun. 2003.

[2] F. Hartung and F. Ramme, "Digital right management and watermarking of multimedia content for m-commerce applications," *IEEE Commun. Mag.*, vol. 38, no. 11, pp. 78–84, Nov. 2000.

[3] I. J. Cox, J. Kilian, F. T. Leighton, and T. Shamoon, "Secure spread spectrum watermarking for multimedia," *IEEE Trans. Image Process.*, vol. 6, no. 12, pp. 1673–1687, Dec. 1997.

[4] P. T. Yu, H. H. Tsai, and J. S. Lin, "Digital watermarking based on neural networks for color images," *Signal Process.*, vol. 81, pp. 663–671, 2001.

[5] S. H. Wang and Y. P. Lin, "Wavelet tree quantization for copyright protection watermarking," *IEEE Trans. Image Process.*, vol. 13, no. 2, pp. 154–165, Feb. 2004.

[6] I. J. Cox and M. L. Miller, "The first 50 years of electronic watermarking," *J. Appl. Signal Process.*, vol. 2, pp. 126–132, 2002.

[7] S. Mallat, *A Wavelet Tour of Signal Processing*. New York: Academic, 1998.

[8] Q. Sun, N. Bi, and D. Huang, *An Introduction to Multiband Wavelets*. Hangzhou, China: Zhejiang Univ. Press, 2001.

[9] N. E. Huang, Z. Shen, S. R. Long, M. C. Wu, H. H. Shih, Q. Zheng, N.-C. Yen, C. C. Tung, and H. H. Liu, "The empirical mode decomposition and the hilbert spectrum for nonlinear and non-stationary time series analysis," *Proc. Roy. Soc. Lond. A*, vol. 454, pp. 903–995, 1998.

[10] P. Steffen, P. N. Heller, R. A. Gopinath, and C. S. Burrus, "Theory of regular M-band wavelet bases," *IEEE Trans. Signal Process.*, vol. 41, no. 12, pp. 3497–3511, Dec. 1993.

[11] A. K. Soman, P. P. Vaidyanathan, and T. Q. Nguyen, "Linear phase paraunitary filter banks: Theory, factorizations and designs," *IEEE Trans. Signal Process.*, vol. 41, no. 12, pp. 3480–3496, Dec. 1993.

[12] H. Zou and A. H. Tewfik, "Discrete orthogonal M-band wavelet decompositions," in *Proc. IEEE Int. Conf. Acoustics, Speech, and Signal Processing*, 1992, vol. 4, pp. 605–608.

[13] N. Bi, X. Dai, and Q. Sun, "Construction of compactly supported M-band wavelets," *Appl. Comput. Harmon. Anal.*, vol. 6, pp. 113–131, 1999.

[14] S. Oraintara, T. D. Tran, P. N. Heller, and T. Q. Nguyen, "Lattice structure for regular paraunitary linear-phase filterbanksand M-band orthogonal symmetric wavelets," *IEEE Trans. Signal Process.*, vol. 49, no. 11, pp. 2659–2672, Nov. 2001.

[15] P.-L. Shui and Z. Bao, "M-band biorthogonal interpolating wavelets via lifting scheme," *IEEE Trans. Signal Process.*, vol. 52, no. 9, pp. 2500–2512, Sep. 2004.

[16] T. Aydin, Y. Yemez, E. Anarim, and B. Sankur, "Multidirectional and multiscale edge detection via M-band wavelet transform," *IEEE Trans. Image Process.*, vol. 5, no. 9, pp. 1370–1377, Sep. 1996.

[17] Y. Chitre and A. P. Dhawan, "M-band wavelet discrimination of natural textures," *Pattern Recognit.*, vol. 32, pp. 773–789, 1999.

[18] C. Q. Zhu, W. Z. Shi, and G. Wan, "Reducing remote sensing image and simplifying DEM data by the multi-band wavelet," *Int. J. Remote Sens.*, vol. 23, pp. 525–536, 2002.

[19] W.-L. Lee, Y.-C. Chen, and K.-S. Hsieh, "Ultrasonic liver tissues classification by fractal feature vector based on M-band wavelet transform," *IEEE Trans. Med. Imag.*, vol. 22, no. 3, pp. 382–392, Mar. 2003.

[20] M. K. Kundu and M. Acharyya, "M-Band wavelet: Application to texture segmentation for real life image analysis," *Int. J. Wavelets, Multires., Inf. Process.*, vol. 1, pp. 115–149, 2003.

[21] L. Shen and Q. Sun, "Bi-orthogonal wavelet system for high-resolution image reconstruction," *IEEE Trans. Signal Process.*, vol. 52, no. 7, pp. 1997–2011, Jul. 2004.

[22] K. Prayoth, A. Kitti, and S. Arthit, "A new approach for optimization in image watermarking by using genetic algorithms," *IEEE Trans. Signal Process.*, vol. 12, no. 12, pp. 4707–4719, Dec. 2005.

[23] M. S. Hsieh, D. C. Tseng, and Y. H. Huang, "Hiding digital watermarks using multiresolution wavelet transform," *IEEE Trans. Ind. Electron.*, vol. 48, no. 5, pp. 875–882, Oct. 2001.

[24] G. Lahouari, B. Ahmed, K. I. Mohammad, and B. Said, "Digital image watermarking using balanced multiwavelets," *IEEE Trans. Signal Process.*, vol. 54, no. 4, pp. 1519–1536, Apr. 2006.

[25] T. M. Ng and H. K. Garg, "Maximum-likelihood detection in DWT domain image watermarking using Laplacian modeling," *IEEE Signal Process. Lett.*, vol. 12, no. 4, pp. 345–348, Apr. 2005.
[26] P. Bao and X. Ma, "Image adaptive watermarking using wavelet domain singular value decomposition," *IEEE Trans. Circuits Syst. Video Technol.*, vol. 15, no. 1, pp. 96–102, Jan. 2005.
[27] B. Liu, S. Riemenschneider, and Y. Xu, "Gearbox fault diagnosis using empirical mode decomposition and hilbert spectrum," *Mech. Syst. Signal Process.*, vol. 20, pp. 718–734, 2006.
[28] J. C. Nunes, Y. Bouaoune, E. Delechelle, O. Niang, and Ph. Bunel, "Image analysis by bidimensional empirical mode decomposition," *Image Vis. Comput.*, vol. 21, pp. 1019–1026, 2003.
[29] H. Liang, S. L. Bressler, R. Desimone, and P. Fries, "Empirical mode decomposition: A method for analyzing neural data," *Neurocomputing*, vol. 65-66, pp. 801–807, 2005.
[30] D. Yu, J. Cheng, and Y. Yang, "Application of EMD method and hilbert spectrum to the fault diagnosis of roller bearings," *Mech. Syst. Signal Process.*, vol. 19, pp. 259–270, 2005.
[31] R. W. Suter, *Multirate and Wavelet Signal Processing*. New York: Academic, 1998.
[32] I. Daubechies, "Ten lectures on wavelets," presented at the Regional Conf. Ser. Applied Mathematics, 1992.
[33] N. Bi and D. Huang, "A class of orthogonal and symmerric 4-band wavelets with one-parameter," *Chin. J. Numer. Math. Appl.*, vol. 27, pp. 15–26, 2005.
[34] C.-Y. Lin, M. Wu, J. A. Bloom, I. J. Cox, M. L. Miller, and Y. M. Lui, "Rotation, scale, and translation resilient watermarking for images," *IEEE Trans. Image Process.*, vol. 10, no. 5, pp. 767–782, May 2001.
[35] X. Kang, J. Huang, Y.-Q. Shi, and Y. Lin, "A DWT-DFT composite watermarking scheme robust to affine transform and JPEG compression," *IEEE Trans. Circuits Syst. Video Technol.*, vol. 13, no. 8, pp. 776–786, Aug. 2003.

Ning Bi received the B.Sc. and Ph.D. degrees in mathematics from Zhejiang University, China, in 1989 and 2002, respectively.

He is currently with Department of Scientific Computing and Computer Applications and the Guangdong Key Laboratory of Information Security Technology, Sun Yat-Sen University, Guangzhou, China. He has published more than 20 papers and authored the book *An Introduction to Multiband Wavelets* with Q. Sun and D. Huang. His research interests include multiband wavelets, watermarking, and signal processing.

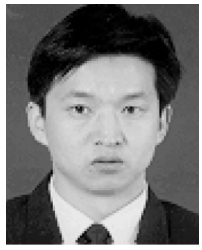

Qiyu Sun received the B.Sc. and Ph.D. degrees in mathematics from Hangzhou University, China, in 1985 and 1990, respectively.

He is currently with Department of Mathematics, University of Central Florida, Orlando. He held prior positions with the Zhejiang University, China; the National University of Singapore; Vanderbilt University, Nashville, TN; and the University of Houston, Houston, TX. He has published more than 80 papers and authored the book *An Introduction to Multiband Wavelets* with N. Bi and D. Huang. His research interest include multiband wavelets, sampling theory, wavelet and frame theory, and Fourier analysis.

Dr. Sun is the Editor of the *Journal of Advances in Computational Mathematics*.

Daren Huang received the B.S. and M.S. degrees in mathematics from Zhejiang University, China, in 1968 and 1981, respectively.

He is currently a Professor with the School of Mathematics and Computing Science, Sun Yat-Sen University, Guangzhou, China. He has published more than 120 papers and two books. His research interests include approximation theory, wavelets, signal processing, image processing, and information security.

Zhihua Yang received the M.S. degree in automation from Hunan University, China, and the Ph.D. degree in computer science from Sun Yat-sen University, Guangzhou, China, respectively, in 1995 and 2005.

He is currently an Associate Professor with the Information Science School, GuangDong University of Business Studies, Guangzhou, China. His research interests include signal analysis, pattern recognition and image processing.

Jiwu Huang received the B.S. degree from Xidian University, China, in 1982, the M.S. degree from Tsinghua University, China, in 1987, and the Ph.D. degree from the Institute of Automation, Chinese Academy of Sciences, in 1998.

He is currently a Professor with the School of Information Science and Technology, Sun Yat-Sen University, China. His current research interests include multimedia security and data hiding.

Dr. Huang serves as a member of IEEE CASS Technical Committee of Multimedia Systems and Applications.